



This is a repository copy of *Revealing the role of the constant phase element in relaxor ferroelectrics*.

White Rose Research Online URL for this paper:
<https://eprints.whiterose.ac.uk/182600/>

Version: Published Version

Article:

Vendrell, X., Ramírez-González, J., Ye, Z.-G. et al. (1 more author) (2022) Revealing the role of the constant phase element in relaxor ferroelectrics. *Communications Physics*, 5 (1). 9.

<https://doi.org/10.1038/s42005-021-00775-1>

Reuse

This article is distributed under the terms of the Creative Commons Attribution (CC BY) licence. This licence allows you to distribute, remix, tweak, and build upon the work, even commercially, as long as you credit the authors for the original work. More information and the full terms of the licence here:
<https://creativecommons.org/licenses/>

Takedown

If you consider content in White Rose Research Online to be in breach of UK law, please notify us by emailing eprints@whiterose.ac.uk including the URL of the record and the reason for the withdrawal request.



eprints@whiterose.ac.uk
<https://eprints.whiterose.ac.uk/>

Revealing the role of the constant phase element in relaxor ferroelectrics

Xavier Vendrell ^{1,3}, Julia Ramírez-González ¹, Zuo-Guang Ye ²✉ & Anthony R. West ¹✉

Relaxor ferroelectrics exhibit both static and dynamic local structural order which controls their frequency-dependent electrical properties. A combination of advanced scattering and microscopy techniques have been used recently to determine the local structure of relaxors. To complement these, here we show an approach to electrical property measurements which identifies local dipoles whose switching is co-operative, temperature-dependent and responsible for the observed dispersion in dielectric properties. Impedance measurements and equivalent circuit analysis of a canonical relaxor, $\text{Pb}(\text{Mg}_{1/3}\text{Nb}_{2/3})\text{O}_3$ single crystal, over the ranges 180–1050 K and 100 Hz–1 MHz, show that incorporation of a single constant phase element into the equivalent circuit used to fit experimental data is able to account fully for the dispersions that characterise the relaxor response, over this frequency range. This allows parametrisation of the relaxor behaviour, gives increased understanding of the relaxation mechanisms responsible and forms the basis for modifying and controlling relaxor characteristics.

¹University of Sheffield, Department of Materials Science & Engineering, Mappin St, Sheffield S1 3JD, UK. ²Department of Chemistry and 4D LABS, Simon Fraser University, 8888 University Drive, Burnaby, B.C. V5A 1S6, Canada. ³Present address: Institute of Energy Technologies, Department of Chemical Engineering and Barcelona Research Center in Multiscale Science and Engineering, Universitat Politècnica de Catalunya, Escola d'Enginyeria de Barcelona Est (EEBE), Eduard Maristany 10-14, 08019 Barcelona, Spain. ✉email: zye@sfu.ca; a.r.west@sheffield.ac.uk

Pb(Mg_{1/3}Nb_{2/3})O₃ (PMN) is one of the most extensively studied relaxor ferroelectric materials, due to its high permittivity and frequency dispersion over a wide temperature range¹. The sharp permittivity maximum observed at certain temperatures in normal ferroelectrics such as BaTiO₃, is associated with a ferroelectric-paraelectric phase transition². In PMN, local structural order within the average, randomly-distributed arrangement of Mg²⁺ and Nb⁵⁺ cations on the octahedral B-sites of the perovskite structure is believed to produce chemically ordered regions (CORs) as well as polar defects that lead to the formation of polar nano-regions (PNRs)³ below the characteristic Burns temperature, T_B , ~620 K⁴. The presence of PNRs is held responsible for the frequency-dependent dielectric properties that are characteristic of relaxors^{5–7}. To explain the nature of the interactions between local polarisation and the mechanism of relaxor behaviour, several models have been proposed^{8–10}.

Measurement of the electrical properties of PMN and other relaxors is usually carried out by dielectric spectroscopy (DS), involving fixed frequency sweeps of real and imaginary permittivity, ϵ' , ϵ'' and dielectric loss, $\tan \delta$ as a function of temperature. The permittivity data pass through broad maxima whose positions and magnitude, characterized by temperature (T_{\max}) and permittivity (ϵ'_{\max}) are frequency-dependent. Typically, the maxima are not associated with any structural phase transition⁴, which is in contrast to the first-order ferroelectric phase transitions observed in materials such as BaTiO₃ whose dielectric maxima are sharp and frequency-independent.

Despite intensive studies in recent decades, it is still a challenge to describe fully the peculiar, frequency-dependent dielectric response of relaxors. Since the dielectric data are usually collected at fixed frequencies, equivalent circuit analysis to identify and quantify resistive and capacitive circuit elements is not feasible. DS is a well-established method for the analysis of materials that are both electrical insulators and show local dipolar reorientation processes, but for conducting materials, impedance spectroscopy (IS), which adopts an alternative approach to data collection and analysis, is used. IS involves variable frequency, fixed temperature data collection, from which, for example, ϵ' and ϵ'' data can also be obtained. IS methodology involves several stages including data collection using frequency sweep at fixed temperatures; inspection of the data to establish the most appropriate equivalent circuit, followed if necessary by accurate circuit fitting; extraction of resistive, capacitive (and inductive) circuit component values, often as a function of temperature; finally, assignment of these circuit parameters to the electrical properties of the material.

In the relaxor literature, the vast majority of publications use DS procedures and methodology. A few impedance studies on PMN have been reported^{11–13} but contain no detailed circuit analyses, nor identification and quantification of the parameters that control the relaxor response. Here, we show that the use of variable frequency, fixed temperature IS measurements and analysis of a PMN single-crystal allow identification of an equivalent circuit that contains a constant phase element (CPE) in series with a blocking capacitance. Together, these control the temperature and frequency dependence of ϵ' that is the fundamental characteristic of relaxor behavior. These measurements provide much insight into understanding relaxor phenomena by quantifying the dispersive permittivity data in terms of the frequency (and temperature) - dependent resistive and capacitive components which make up the CPE. They provide a basis for future work to gain an improved understanding of the effects of composition, processing conditions, temperature and voltage on the properties of PMN and other relaxors.

Results and discussion

Proposed equivalent circuit. The equivalent circuit that is found to model the impedance response of single-crystal PMN is

derived from a series combination of a resistor and capacitor, which is a standard idealised circuit used to represent dielectric relaxation processes, Fig. 1a. Capacitance C_1 represents the limiting high frequency, and frequency-independent, capacitance or bulk permittivity of the sample. Elements R_1 and C_2 represent the ionic motions that give rise to dielectric relaxation: R_1 is a measure of the resistance to the ionic motions and C_2 gives the amount of charge stored as a result of the polarisation. In relaxors, however, the ionic displacements, especially of Pb²⁺ ions, are linked co-operatively with the displacements of other cations and anions, which means that single-valued, idealised, frequency-independent R and C parameters cannot adequately represent the 'real' response. Consequently, the circuit requires modification by the inclusion of frequency-dependent circuit elements. In particular, it is found that replacement of R_1 by a constant phase element, CPE₁ gives a circuit, Fig. 1b that accurately fits the frequency-dependence of dielectric and impedance properties.

The resulting parametrisation allows the description of the relaxor response in terms of a small number of quantifiable parameters. This eliminates the need for the empirical distributions of relaxation times that have, variously, been used to fit the characteristic dispersions in permittivity and dielectric loss¹⁴, but more importantly, the equivalent circuit parameters and their temperature dependence, including the CPE, provide a way to describe, parametrise and understand relaxor behavior.

Experimental data

Dielectric spectroscopy results. Dielectric spectroscopy measurements of the temperature dependence of ϵ' and ϵ'' of a (100)-oriented PMN single crystal at five different frequencies are shown in Fig. 2a. Both ϵ' and ϵ'' show diffuse peaks, similar to those reported previously for PMN¹⁴, whose temperatures, T_{\max} , increase with frequency. The magnitude of ϵ'_{\max} decreases with frequency whereas that of ϵ''_{\max} increases. These data, and their temperature dependence, are typical of PMN single crystals, PMN ceramics and a wide range of other relaxor materials. The main parameters that can be extracted from such data sets are relaxation times corresponding to the temperatures and frequencies of the permittivity maxima and the onset temperature of the deviation from the high-temperature Curie-Weiss law in ϵ' which is identified as the Burns temperature.

Impedance spectroscopy results. Impedance spectroscopy data for the same sample were obtained from variable frequency measurements at fixed temperatures. Presentation of the data as an

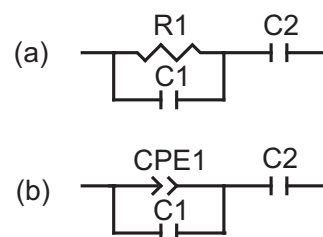


Fig. 1 Equivalent circuits used to represent dielectric relaxation

processes. a Resistance R_1 in series with Capacitance C_2 represents the motions that give rise to dielectric relaxation: R_1 is a measure of the resistance to the ionic motions and C_2 gives the amount of charge stored as a result of the polarisation. Capacitance C_1 in parallel with R_1 represents the limiting high frequency, and frequency-independent, capacitance or bulk permittivity of the sample. **b** R_1 is substituted by a constant phase element CPE₁, which is a frequency-dependent circuit element and represents the frequency-dependent polarisation processes.

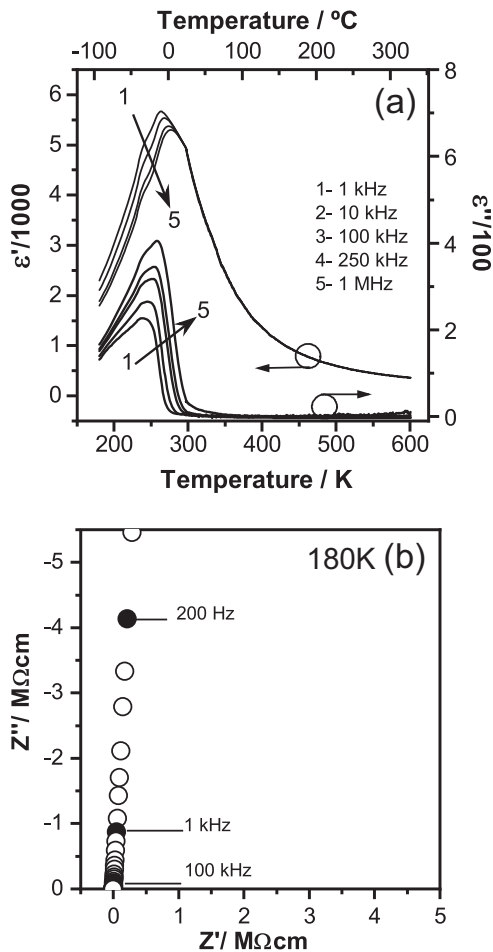


Fig. 2 Dielectric and impedance spectroscopy measurements of $\text{Pb}(\text{Mg}_{1/3}\text{Nb}_{2/3})\text{O}_3$ single crystal. **a** Temperature dependence of the real and imaginary parts of the relative permittivity measured at different frequencies and **b** impedance complex plane plot at 180 K for the $\text{Pb}(\text{Mg}_{1/3}\text{Nb}_{2/3})\text{O}_3$ single crystal.

impedance complex plane plot (Z'' vs Z') is shown for one temperature, 180 K, in Fig. 2b. A spike is seen which passes through the origin at high frequencies. The spike represents a blocking capacitance that is in parallel with a very large resistance whose value is too large to measure. This confirms that there is no leakage of current through the capacitor: a finite-valued resistance in parallel with the capacitance would convert the spike into a low-frequency semicircle of diameter equal to the resistance value. There is no evidence of any curvature in the spike, even at the lowest frequencies and therefore, the parallel resistance for the data set in Fig. 2b would have a value of at least 100 MΩcm, which indicates high quality of the PMN crystal.

A characteristic feature of impedance complex plane plots on linear scales such as Fig. 2b is that they give preferential weighting to the most resistive component in the electrical make-up of the system under study and may be completely insensitive to lower impedance, ac effects¹⁵. In order to obtain a weighting-free overview of the sample impedance over the entire frequency spectrum, it is necessary to use alternative methods of data processing and analysis, specifically by utilising the transformations encapsulated by Eqs. (1–3)^{16,17}. Impedance (Z^*) data were therefore corrected for overall geometry and converted to permittivity (ϵ^*), admittance (Y^*) and electric modulus (M^*)

formalisms^{16,17}:

$$Z^* = Z' - jZ'' = (Y^*)^{-1} \quad (1)$$

$$M^* = M' - jM'' = j\omega C_0 Z^* \quad (2)$$

$$\epsilon^* = \epsilon' - j\epsilon'' = (M^*)^{-1} \quad (3)$$

where ω is the angular frequency, $2\pi f$ and C_0 is the vacuum capacitance of the measuring cell and electrodes with an air gap in place of the sample¹⁵. The analysis method that was found to be most suitable here was to present the data in two additional formats, capacitance (C') vs log frequency and log real part of the admittance (Y') vs log frequency¹⁵, as shown in Fig. 3.

Figure 3a, b shows capacitance, C' data extracted from impedance measurements at low temperatures, 180–290 K; this includes transformation of the 180 K data set shown in Fig. 2b. Over the frequency range 10^2 – 10^6 Hz, C' data are frequency-dependent up to 280 K. C' increases with both increasing temperature and decreasing frequency up to 260 K but starts to decrease at higher temperatures. At 270 and 280 K, Fig. 3b, C' data are constant at low frequencies but frequency-dependent at high frequencies, showing that the frequency-independent behaviour extends to increasingly higher frequencies with increasing temperature. At and above ~ 290 K, C' data are independent of frequency over the entire measured range and decrease with increasing temperature up to at least 575 K, Fig. 3c. This decrease is consistent with the decrease in ϵ' data at higher temperatures shown in Fig. 2a.

Admittance Y' data, are also frequency-dependent over the entire temperature, 180–290 K and frequency ranges, Fig. 3d, e. On the log-log scales shown, this ac conductivity, Y' data give an approximately linear, power-law dependence with, for example, slope $n \sim 0.88$ at 220 K, that gradually increases with decreasing temperature towards a value approaching unity at 180 K. Above ~ 275 K, Y' decreases, especially at low frequencies (Fig. 3e) and departs from the linear power-law behaviour seen at higher frequencies and lower temperatures. Above ~ 300 K, the Y' data were noisy and values were too small to be measured with any accuracy; essentially, such data corresponded to the internal impedance of the measuring equipment (not shown).

Equivalent circuit analysis. As the first step in data and circuit analysis, an inspection of the plots in Fig. 3 indicates that:

- (i) Over the frequency range 100 Hz–1 MHz and above ~ 290 K, C' is frequency-independent but temperature-dependent. This frequency-independence, Fig. 3b, c and the increasing difficulty in obtaining Y' data above 300 K, Fig. 3e, indicate a capacitive response with very little leakage conductivity. These high-temperature data can therefore be represented by a single, ideal capacitor.
- (ii) A small amount of ac conductivity is seen at lower temperatures and takes the form of a power-law response of the Y' data, ≤ 250 K, Fig. 3d. However, the same low-temperature data plotted as C' vs log f , Fig. 3a, b, do not give a power-law response that would be the Kramers-Kronig analogue of the Y' data, which may be expected if the equivalent circuit consisted of a single CPE. Instead, it is clear that the inclusion of an extra circuit element is needed to fit the data.

These observations point to an equivalent circuit that requires a series combination of a capacitor and a constant phase element, Fig. 4a. We find that this circuit fits accurately the impedance data obtained over the limited frequency range 10^2 – 10^6 Hz, in all

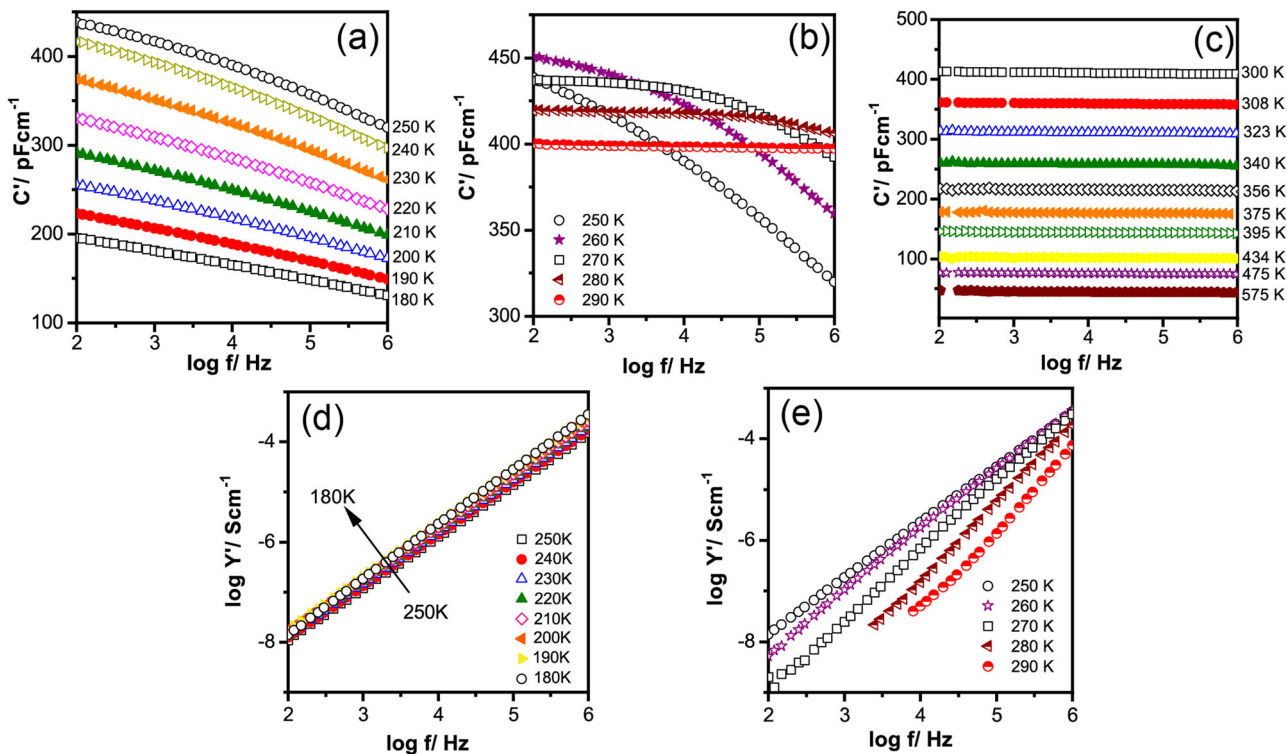


Fig. 3 Impedance data of $\text{Pb}(\text{Mg}_{1/3}\text{Nb}_{2/3})\text{O}_3$ single crystal at different temperatures plotted as capacitance C' and admittance Y' . Capacitance C' as a function of frequency at **a** 180–250 K, **b** 250–290 K, **c** 300–575 K, admittance Y' as a function of frequency at **d** 180–250 K and **e** 250–290 K, for the PMN single crystal.

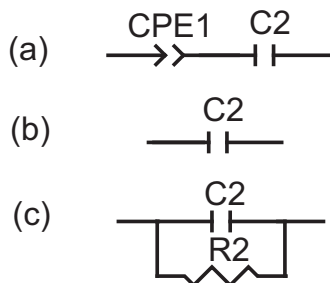


Fig. 4 Representation of impedance response. The impedance response of $\text{Pb}(\text{Mg}_{1/3}\text{Nb}_{2/3})\text{O}_3$ single crystal was represented as follows; **a** for temperatures below ~310 K, where frequency-dependent relaxor response is observed, a constant phase element CPE_1 in series with a capacitor C_2 was used. It can be noted that capacitor C_1 from Fig. 1b was not included because its contribution is very limited for the temperature and frequency ranges over which impedance data were collected. **b** Between ~300 and 800 K, the circuit simplifies to capacitance C_2 , as the response is frequency-independent and entirely capacitive, with no evidence of measurable *ac* or *dc* conductivity. **c** Above ~800 K the material behaves as a leaky dielectric, with no anomalous dielectric response, and is represented ideally by a single parallel element, R_2C_2 , in which the leakage resistance R_2 is in parallel with capacitance C_2 .

formalisms, for temperatures below 275 K, as shown for C' and Y' at two temperatures, 250 K in Fig. 5a, b and 270 K in Fig. 5c, d. In particular, it accounts for the frequency-dependence of C' Fig. 5a, c.

At higher temperatures, ~300–575 K, the equivalent circuit, over the measured range of frequencies, reduces to a single capacitor, Fig. 4b, because C' data were frequency-independent, Fig. 3b, c and Y' data were too small to be measured.

A CPE takes the form:

$$Y^* = A\omega^n + jB\omega^n = Y' + jY'' \tag{4}$$

where $j = \sqrt{-1}$ and A, B and n are inter-related by:

$$A/B = \tan n\pi/2 \tag{5}$$

A CPE may be regarded as a parallel combination of a resistor, Y' and capacitor, Y'' that are both frequency-dependent admittances and whose relative contributions are given by the parameter n . If $n = 0$, the resistive component of Eq. (4) reduces to an ideal resistor, $Y' = A$; if $n = 1$, the capacitive component reduces to an ideal capacitor, $Y'' = \omega B$. For intermediate values of n , the CPE has the characteristics of a parallel RC element but with frequency-dependent R and C values.

From the fits to circuit (Fig. 4a) at low temperatures, 180–290 K, the values of the circuit parameters, A_1, B_1, n_1 and C_2 were extracted and are shown as a function of temperature in Fig. 6. A_1 and B_1 increase slightly with temperature up to 250 K and much more rapidly at higher temperatures (Fig. 6b). At the same time, with increasing temperature, n_1 decreases slightly at lower temperatures but much more rapidly above 250 K. Capacitance C_2 passes through a maximum at 250 K, with value ~500 pFcm⁻¹ that corresponds to permittivity of ~5500, using the relation

$$C = \epsilon_0 \epsilon' A l^{-1} \tag{6}$$

where ϵ_0 is the permittivity of free space, 8.854×10^{-14} Fcm⁻¹.

At much higher temperatures, >800 K, the PMN crystal started to show a small amount of leakage conductivity and its impedance data gave a single, almost semicircular, arc in the Z^* complex plane, Fig. 7a. The temperature dependence of the resistance obtained from the low-frequency intercept on the Z' axis, plotted in Arrhenius format, Fig. 7b shows a linear response

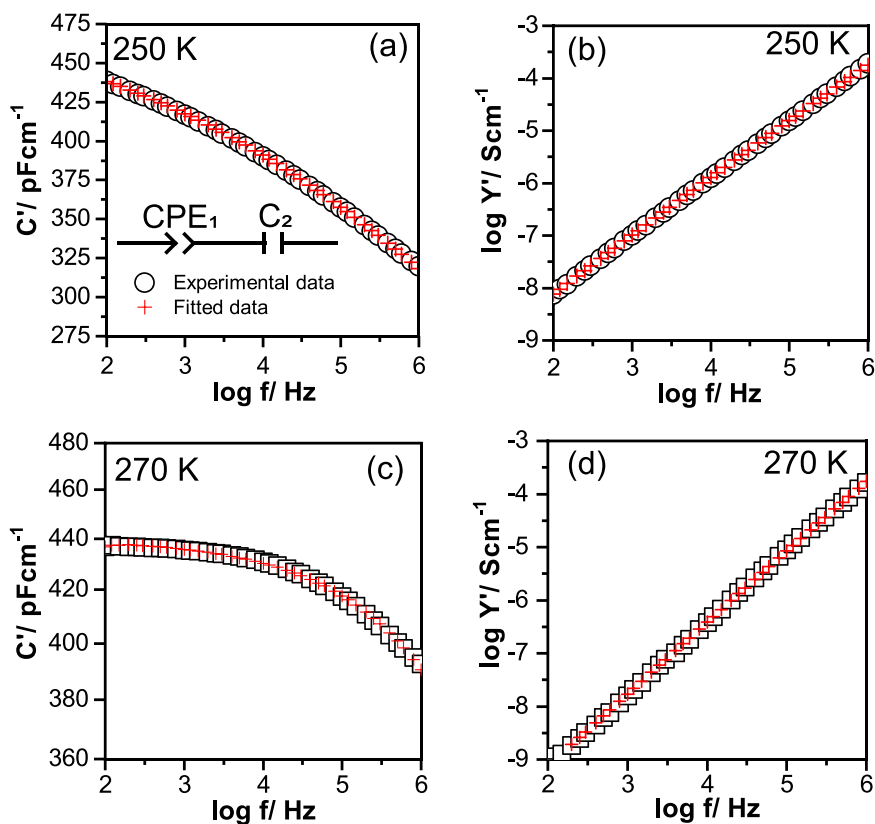


Fig. 5 Capacitance C' and conductivity Y' as a function of frequency. Experimental data and fitted simulations of equivalent circuit Fig. 4a as a function of frequency at 250 K for **a** C' , **b** Y' and at 270 K for **c** C' and **d** Y' , for the $\text{Pb}(\text{Mg}_{1/3}\text{Nb}_{2/3})\text{O}_3$ single crystal. Comments on errors are given in the Methods section (impedance spectroscopy measurements).

with activation energy $E_a = 1.56(3)$ eV, similar to that reported previously¹⁷.

The impedance of single-crystal PMN may be separated into three temperature ranges:

- (i) below ~ 310 K, where frequency-dependent relaxor response is observed. The impedance data fit a modified series RC equivalent circuit, Fig. 4a, in which frequency-dependent CPE_1 replaces the resistor R_1 .
- (ii) over the range ~ 310 – 800 K, the response is entirely capacitive with no evidence of measurable ac or dc conductivity. The circuit simplifies to capacitance C_2 , Fig. 4b.
- (iii) at temperatures above 800 K, a small leakage conductivity with activation energy $1.56(3)$ eV is measured. At these high temperatures, the material is simply a leaky dielectric, with no anomalous dielectric response, and is represented ideally by a single parallel element, R_2C_2 , Fig. 4c, in which the leakage resistance R_2 is in parallel with capacitance C_2 . No further discussion of these high-temperature data is given.

The circuit shown in Fig. 1b includes a high-frequency capacitance, C_1 , not present in Fig. 4a. This is because its contribution is very limited for the temperature and frequency ranges over which impedance data were collected. In order to see evidence of C_1 , for instance in plots of C' vs $\log f$ such as Fig. 3a, b, it would be necessary to extend the measurements to higher frequency and/or lower temperature; under these conditions, the C' data would level off to a frequency-independent plateau at high frequencies. The presence of C_1 is important for understanding the full range of relaxor behaviour even though it was not observed in these particular data sets.

The complete relaxor response of a homogeneous PMN single crystal for frequencies from *dc* up to at least 1 MHz can be quantified in terms of four variables, the A_1 , n_1 parameters of CPE_1 and the capacitances C_1 and C_2 . Circuit Fig. 1b is a dielectric circuit. It contains a CPE which represents the frequency-dependent polarisation processes. These processes are in series with a blocking capacitance, C_2 . Assignment of the four variables to the impedance characteristics of the sample, and their significance, is as follows:

Element C_2 passes through a broad maximum, Fig. 6a with a permittivity of ~ 5800 at ~ 250 K. It is attributed to the sample permittivity that is associated with the low-frequency limit of the frequency-dependent polarisation processes. Data for C_2 correspond to the values that would be obtained by zero frequency LCR measurements, as indicated in Fig. 8.

For the sets of data between ~ 180 and 350 K, dispersions in ϵ' and ϵ'' are seen, Fig. 2a. To account for these dispersions, the experimental C' data include a contribution from the variable resistor/capacitor combination in series with C_2 that is represented by CPE_1 . The n parameter of CPE_1 determines the relative contributions of the resistive and capacitive components to the CPE.

When $n = 1$, a CPE is purely capacitive. Data in Fig. 6a show that at low temperatures, $n = \sim 0.9$ and the parallel resistive component of the CPE is very large, but not infinite, as shown by the small value of A_1 in Fig. 6b. With increasing temperature, A_1 increases, especially above 250 K and n decreases to ~ 0 by 300 K at which point, the CPE is purely conductive.

The entire relaxor response of the PMN crystal can therefore be represented by inclusion of a constant phase element in the series RC equivalent circuit of a dielectric. This allows the

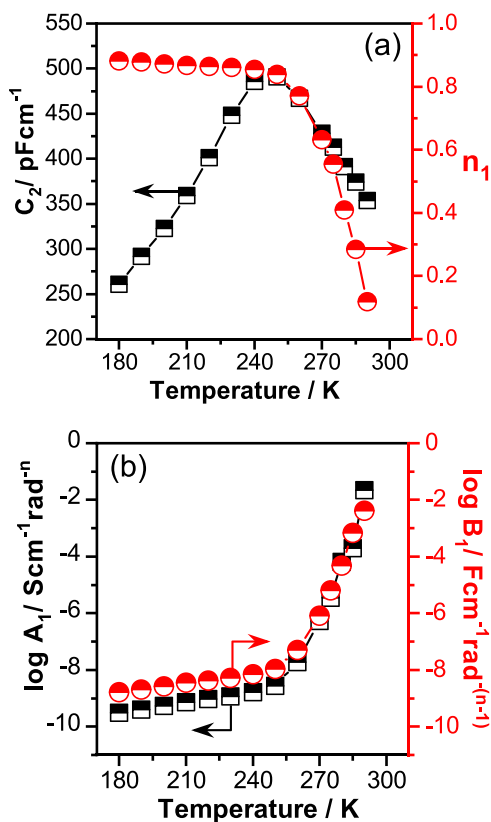


Fig. 6 Temperature dependence of equivalent circuit fitting parameters. Results for **a** n_1 , C_2 and **b** A_1 , B_1 between 180 and 290 K for the $\text{Pb}(\text{Mg}_{1/3}\text{Nb}_{2/3})\text{O}_3$ single crystal. Errors are within the size of the data points; see Methods section (impedance spectroscopy measurements).

temperature- and frequency-dependence of the dielectric response to be quantified in terms of three parameters: A_1 , n_1 of CPE_1 and the series capacitance C_2 . The nature of the CPE, given by the value of n_1 , changes from mainly capacitive at temperatures below the permittivity maximum, ~ 250 K, to increasingly conductive at higher temperatures. At the same time, the ac conductivity increases by more than six orders of magnitude.

Experimental data were limited to 1 MHz. At higher frequencies, it is anticipated that the C' data would level off at the value C_∞ , represented by C_1 in Fig. 1b. C_1 represents the high-frequency limit of the ionic polarisation processes responsible for the bulk permittivity whereas C_2 represents their low-frequency limit. Circuit Fig. 1b represents dielectric relaxation in which cooperative polarisation processes are involved; these are represented by the CPE.

The temperature dependence of A_1 , the ac conductivity parameter, controls the time constant (τ) for charging capacitor C_2 , which is given by $\tau = A_1^{-1}C_2$ and $\omega\tau = 1$. At large values of A_1 , τ is small and the relaxation frequency, ω is very large, $\gg 1$ MHz. C_2 is fully charged, therefore and C' is independent of smaller measuring frequencies, Fig. 3c. Below ~ 300 K, A_1 decreases very rapidly, Fig. 6b, which is reflected in the increasing frequency dependence of C' , Fig. 3a, b. Below ~ 250 K, the ionic motions responsible for the rapid change in A_1 at higher temperatures cease, but nevertheless, there is still a small temperature dependence of A_1 at lower temperatures, Fig. 6b.

Comparison with the literature. The existence of A_1 and the nature of its temperature dependence imply that short-range ionic displacements are responsible for the high-frequency ac

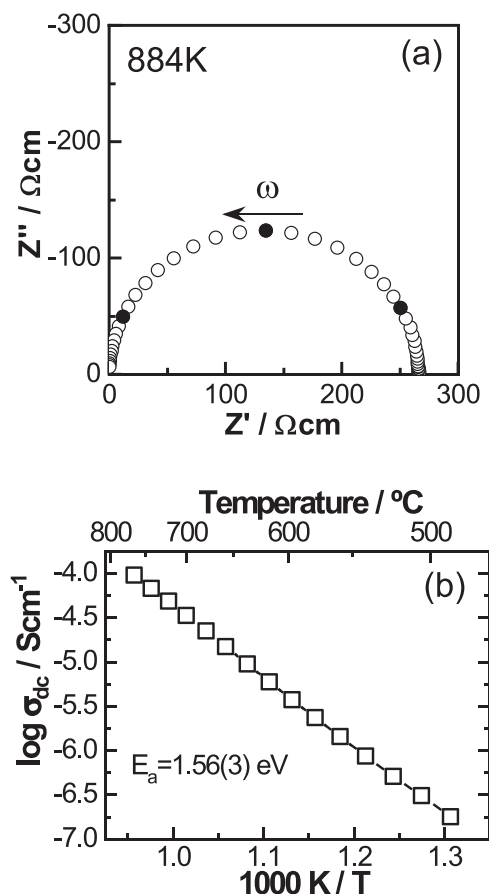


Fig. 7 High-temperature impedance data showing evidence of leakage conductivity above 800 K. **a** Impedance complex plane plot at 884 K and **b** Arrhenius plot for the resistance of $\text{Pb}(\text{Mg}_{1/3}\text{Nb}_{2/3})\text{O}_3$ single crystal.

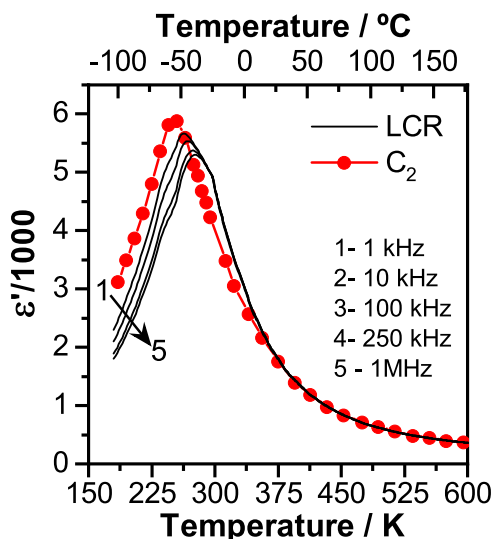


Fig. 8 Temperature dependence of the real part of the permittivity obtained by impedance and dielectric spectroscopy. The LCR data were obtained by fixed frequency measurement. The C_2 data were obtained by fitting variable frequency impedance data.

conductivity, consistent with current thinking on the local nano-structural ordering in Pb-based relaxors such as PMN. There is much recent evidence from a combination of diffuse- and total-scattering studies and scanning transmission electron microscopy

combined with high-angle annular dark-field imaging (HAADF) that Pb^{2+} ions are responsible for the PNRs in lead-based relaxors and relaxor ferroelectrics^{18–23}. The Pb displacements, off-centre from the 12-coordinate A-site in the perovskite structure, are non-random in the $\langle 111 \rangle$ directions. Each PNR has a preferred displacement direction that is different from that in adjacent PNRs, giving rise, on a larger scale, to aggregate PNRs with several inequivalent $\langle 111 \rangle$ clusters. In addition, the Pb displacements are greatest in the PNR centres and decrease outwards, with a smooth cross-over between adjacent PNRs. The Pb displacements are temperature-dependent with a suggestion from results of acoustic measurements that below a certain temperature, permanent nano-regions form²². Studies of PMN-PT ($\text{Pb}(\text{Mg}_{1/3}\text{Nb}_{2/3})\text{O}_3\text{-PbTiO}_3$) materials showed that composition-dependent A-site displacements which were decoupled from smaller B-site displacements, were key to relaxor behaviour and were distinct from phenomena occurring at the morphotropic phase boundary; a new softening effect was proposed, associated with low angle nanodomain walls²³. The earlier model for relaxors of discrete, ordered domains within a disordered matrix²⁴ is now regarded as incompatible with the recent nano-structured picture¹⁹. The nature of the local order has been investigated in detail using diffuse scattering of X-rays and neutrons and four forms of local order identified²¹. These involve local antiferroelectric correlations, seeded by CORs, as distinct from PNRs; local ferroic order and anion displacements, especially in compositions close to the optimum composition for piezoelectricity.

We interpret the electrical property characteristics derived from our impedance measurements in terms of these recent nano-structural studies, as follows. A_1 is a measure of local displacement of Pb^{2+} ions, probably by 10–30 pm, but with magnitude dependent on temperature and the position of Pb^{2+} ions within the PNRs. The displacements are correlated and occur easily at the upper-temperature end of the relaxor behaviour. With decreasing temperature, displacements become less easy as A_1 decreases and domain boundaries start to freeze at ~ 250 K when A_1 has a value $\sim 1 \times 10^{-9} \text{ Scm}^{-1}\text{rad}^{-n}$. Below 250 K, A_1 continues to decrease, but much more slowly. This may be due to small, secondary displacements of Pb^{2+} ions, possibly correlated, but within frozen domains. Alternatively, A_1 may represent smaller B-site displacements. This change in A_1 with temperature is accompanied by a change in value of the n parameter from 0.1 at 290 K, indicative of an essentially conductive CPE, to 0.85 at 255 K, indicative of a mainly capacitive CPE, consistent with freezing of the domain boundaries. At lower temperatures, n increases further to 0.9 at 180 K.

These results represent the first time, of which we are aware, that low-frequency dielectric relaxation data to either side of the permittivity maximum have been fitted accurately to an equivalent circuit that enables quantification of the frequency- and temperature-dependent dielectric response in terms of just three circuit parameters. The resulting parametrisation provides a base with which to analyse, interpret and discuss relaxor data in terms of these circuit parameters. Although various empirical functions have been used in the literature to fit the temperature dependence of fixed frequency dielectric data, their physical significance remains unknown and they are not reviewed here. There is, however, previous recognition of power-law components, with some similarity to a CPE, in dielectric relaxation data over certain frequency ranges^{4,14}.

Circuit simulations. We show simulations of capacitance C' and admittance Y' over the frequency range, μHz –1 THz, Fig. 9, and compare these with experimental data over the limited range of 4

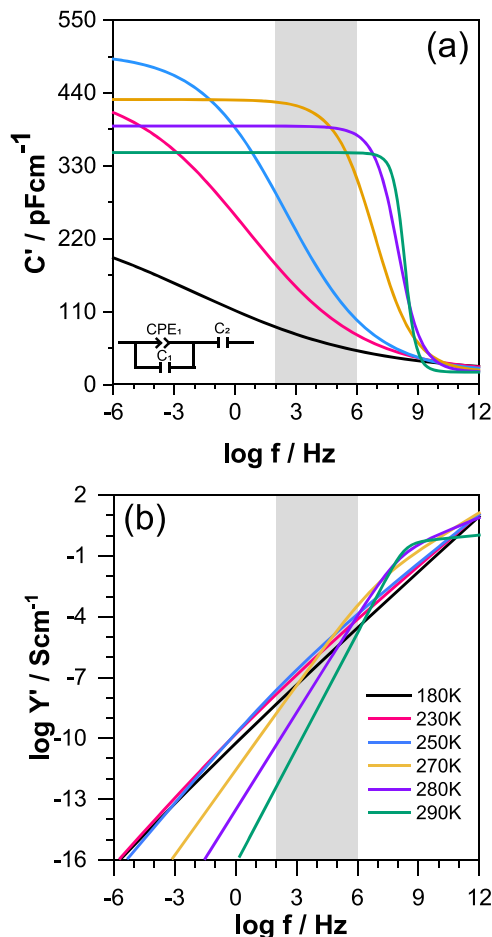


Fig. 9 Equivalent circuit simulations. **a** Capacitance and **b** admittance with increasing temperature, over the frequency range 1 μHz –1 THz of the equivalent circuit shown in inset **a**. The constant phase element CPE_1 represents the frequency-dependent polarisation processes, C_2 is a blocking capacitance that represents the amount of charge stored as a result of the polarisation, and C_1 , the limiting high frequency, and frequency-independent, capacitance of the sample. The shaded region shows the 4 decades of frequency used for the experimental measurements.

Table 1 Simulation values used to generate Fig. 9.

T (K)	A_1 ($\text{Scm}^{-1}\text{rad}^{-n}$)	B_1 ($\text{Fcm}^{-1}\text{rad}^{-(n-1)}$)	n_1	C_1 (pFcm^{-1})	C_2 (pFcm^{-1})
180	3×10^{-10}	2.10×10^{-10}	0.90	20	260
230	1×10^{-9}	7.28×10^{-10}	0.85	20	450
250	3×10^{-9}	2.27×10^{-9}	0.80	20	500
270	5×10^{-7}	4.29×10^{-7}	0.60	20	430
280	5×10^{-5}	4.68×10^{-5}	0.40	20	390
290	1×10^{-2}	9.96×10^{-3}	0.10	20	350

Parameters A_1 , B_1 and n_1 correspond to element CPE_1 ; C_1 , C_2 are capacitances in the circuit shown in Fig. 9a.

decades of frequency, Fig. 9, shaded region. Equivalent circuit Fig. 1b and values shown in Table 1 were used to generate Fig. 9. A_1 , B_1 , n_1 and C_2 values were based on experimental data obtained from Fig. 6, and for illustrative purposes, C_1 was set to 20 pFcm^{-1} .

Simulated capacitances present three distinctive regions, Fig. 9a. At low frequencies, a plateau is observed which corresponds to C_2

and whose frequency domain extends to higher frequencies with increasing temperature. At intermediate frequencies, a frequency-dependent region appears and is related to the presence of a CPE whose frequency domain decreases with temperature. Finally, at the highest frequencies, a plateau whose value approximates to C_1 is observed and may be associated with the contribution of B_1 and C_1 . Simulated admittances present two regions, Fig. 9b. The change in slope of these regions can be related to A_1 and n_1 . The simulated data between 100 Hz and 1 MHz resemble the experimental data shown in Fig. 3.

Models for relaxor behaviour. A widely-accepted model for relaxors involves two components of the dielectric response referred to as ‘flipping’ and ‘breathing’¹⁴ and receives some support from our impedance analyses. ‘Flipping’ refers to dipole reversal processes within the polar nanoclusters that are believed to form below the Burns temperature and is believed to be a high temperature, high frequency process. This implies that flipping is thermally activated, as dipoles change their orientation and we associate this with parameter A_1 of the CPE. In the approximate temperature range of T_{\max} , 250–280 K, the ease of flipping, given by A_1 increases greatly, by 6–7 orders of magnitude, suggesting that the dipolar dynamics become much faster. The temperature dependence of A_1 does not fit Arrhenius behaviour, but is thermally activated down to at least 180 K, Fig. 6b, with a change in temperature dependence at 250 K.

The ‘breathing’ component is attributed to the movement of domain walls in the direction of the applied field at measuring frequencies^{4,14} and is regarded as a low-temperature process. Possibly, this is related to the bulk capacitance, C_1 , whose characterisation was outside our measurement range, but would be observed at a combination of higher frequencies and/or lower temperatures. C_1 is the limiting high-frequency capacitance of the sample, often labelled as C_{∞} , or the ionic polarisation component. With this interpretation, C_1 does not make a significant contribution to relaxor behaviour.

The data analysis methodology presented here using variable frequency, isothermal impedance datasets provides a powerful method to characterise relaxors. Interpretation of temperature-dependent fixed frequency DS data is inherently complicated by the continual, temperature-dependent change in weighting of the equivalent circuit components associated with the CPE at a particular frequency. In addition, fixed frequency DS measurements give snapshot values of permittivities that are not fundamental material properties but instead, are composite values that depend on the measuring frequency. IS data are presented here for one canonical relaxor, PMN single crystal. The frequency-independent parameters n_1 , A_1 and C_2 provide a methodology and basis with which to compare different relaxor materials. From their temperature dependence, fresh insight may be gained into topics such as Volger-Fulcher freezing behaviour and ergodic/nonergodic, or glassy relaxor states, all of which should lead to a better understanding of relaxor phenomena.

The entire relaxor response over the frequency range studied here can be represented by, and simulated using, a simple equivalent circuit in which the key component is a CPE. A CPE is a variable resistance, variable capacitance parallel combination that shows power-law dependence on frequency. Such behaviour is a manifestation of Jonscher’s Law of Universal Dielectric Response^{25–29} that is a ubiquitous feature of the bulk conducting and dielectric properties of a wide range of crystalline and amorphous materials. Prior to the Jonscher’s Law discovery, bulk, high-frequency electrical properties that were frequency-dependent over a limited range of frequencies were commonly modelled by empirical functions that represented distributions of

relaxation times (DRT) and, especially for amorphous materials, attributed to distributions in activation energy. With the realisation of ubiquitous power-law behaviour, and its occurrence in crystalline materials such as single crystal Na beta alumina^{30–33}, it was difficult to conceive how this could be represented by a realistic DRT and distribution of activation energies.

The next major step forward in understanding high-frequency dispersions in electrical properties and power-law behaviour has been their modelling by Almond, Bowen and coworkers^{34–37} in terms of large networks of resistor-capacitor combinations containing many series and parallel connections. This led to the compelling conclusion and demonstration that the CPE n parameter is simply related to the relative number of series and parallel RC connections in the network without the requirement of, for instance, any distribution in activation energies. Effectively, therefore, a CPE gives the frequency response of a large, complex RC network. In the present case, this may be attributed to the co-operative nature of atomic polarisation processes and many body interactions involved in the displacement of Pb atoms in PMN.

The limits of CPE response are when $n = 0$ and $n = 1$. At high temperatures, $n \rightarrow 0$, all the network connections are R-R and effectively the CPE reduces to a small resistance value in series with capacitor C_2 . Hence, there is no frequency dependence in measured C' values. At low temperatures, $n \rightarrow 1$; in the extreme case that $n = 1$, the response is entirely capacitive as all atomic displacements are frozen. This leads to the termination of low-temperature relaxor behaviour in which the permittivity values also become frequency independent.

Many body interactions of the kind suggested here are thought to be responsible for the widely-observed Jonscher Law behaviour in ionically-conducting materials. There are two timescales associated with hopping conduction processes, that associated with individual hops at lattice vibrational frequencies and the much longer timescales associated with long-range conduction for which there is an average residence time of an ion on a particular site between successive hops. Jonscher Law conductivity behaviour effectively covers the range of frequencies between these two-time scales.

To the best of our knowledge, this is the first study of IS measurements and equivalent circuit analysis of a relaxor single crystal in which the bulk properties were studied free from other contributing impedances. Previous studies on a pyrochlore ceramic^{38,39} also reported the key importance of a CPE in explaining relaxor behaviour, but uncertainties over the polycrystalline nature of the samples prevented complete interpretation of the impedance data. However, that work provided the motivation for the single-crystal study reported here.

Methods

Single crystal growth from high-temperature solution. A (100)-oriented $\text{Pb}(\text{Mg}_{1/3}\text{Nb}_{2/3})\text{O}_3$ platelet was prepared using a crystal grown from high-temperature solution⁴⁰. First, MgNb_2O_6 , an intermediate columbite phase for the crystal growth, was prepared by solid-state reaction. For this, stoichiometric amounts of reagent grade MgO (Merck) and Nb_2O_5 (Merck) were mixed, ground and placed in a Pt crucible with a lid. Then, the mixture was heated to 1000 °C for 12 h, with a heating and cooling rate of 100 °C/h. Next, a mixture of MgNb_2O_6 and commercial grade PbO (Johnson-Matthey) was ground. This had 30%wt excess of PbO, as PbO was selected as flux. The mixture was premelted at 1100 °C in a 30 ml Pt crucible filled to $\frac{3}{4}$ of its volume. Following, the crucible lid was sealed by argon-arc welding to prevent (or minimise) the volatilisation of PbO; to equilibrate the internal and atmospheric pressures, a ~ 30 μm hole was drilled through the lid. Then, the sealed crucible was heated to 1300 °C at a heating rate of 100 °C/h, soaked for 5 h and finally cooled slowly at 1 °C/h. Once the temperature reached 950 °C during cooling, the crucible was taken out of the furnace, two holes were bored in the lid and the liquid was decanted. After the crucible was at room temperature the crystals were removed and washed in hot 30% nitric acid to remove any flux residues.

Electrical measurements

Sample preparation for electrical measurements. The platinum paste was applied to opposite (100) faces of the single crystal, dried, decomposed and hardened by heating at 900 °C for 2 h to form electrodes. The crystal was loaded into a conductivity jig inside a non-inductively wound tube furnace.

Dielectric spectroscopy measurements. The dielectric properties were measured using an LCR meter (Agilent E4980 Precision LCR Meter, Agilent Technologies) with an applied voltage of 100 mV, recorded at several frequencies in the range from 1 kHz to 1 MHz. Data points were collected every 60 s from RT to 400 °C at a ramp rate of 1 °C min⁻¹.

Impedance spectroscopy measurements. Impedance spectroscopy (IS) measurements at low temperature (180–320 K, at 10 K intervals) were carried out with an Agilent E4980A (Wokingham, UK) with a measurement accuracy of ±0.05% and an Oxford Cryostat (Abingdon, UK) with Intelligent Temperature Controller (ITC 503 S). At high temperatures (RT – 1023 K), an Agilent 4294A with a measurement accuracy of ±0.08% was used; both sets of measurements covered the frequency range from 100 Hz to 1 MHz. Prior to each set of measurements, the temperature was allowed to stabilise for 30 min. Repeat measurements combined with equivalent circuit analysis showed reproducibility of data with errors in *R* and *C* values, taken from the fitting of complete data sets, of <0.1%.

Open circuit measurements on an empty jig were used to obtain the blank parallel capacitance of the jig and leads, which was subtracted from the values obtained with the sample present in the jig; closed circuit measurements were used to correct for the series resistance of the jig and leads. Data were corrected for the crystal geometry and electrode contact area; therefore, resistivity and permittivity data are reported in units of Ω cm and F cm⁻¹, respectively. Data were analyzed using Zview (Scriber Associates Inc.) software. Impedance (*Z*^{*}) data were corrected for overall geometry and converted to permittivity (ϵ^*), admittance (*Y*^{*}) and electric modulus (*M*^{*}) formalisms using the relations (1–3)^{15,16}.

Data availability

The data used in this study are available from the authors upon reasonable request.

Received: 30 March 2021; Accepted: 25 November 2021;

Published online: 10 January 2022

References

- Cowley, R. A., Gvasaliya, S. N., Lushnikov, S. G., Roessli, B. & Rotaru, G. M. Relaxing with relaxors: a review of relaxor ferroelectrics. *Adv. Phys.* **60**, 229–327 (2011).
- Wada, S. et al. Phase transition behaviors of BaTiO₃–BaZrO₃ solid solutions under high direct current bias fields. *J. Mater. Res.* **17**, 456–464 (2002).
- Cross, L. E. Relaxor ferroelectrics. *Ferroelectrics* **76**, 241–267 (1987).
- Bokov, A. A. & Ye, Z.-G. Recent progress in relaxor ferroelectrics with perovskite structure. *J. Mater. Sci.* **41**, 31–52 (2006).
- Jeong, I.-K. et al. Direct observation of the formation of polar nanoregions in Pb(Mg_{1/3}Nb_{2/3})O₃ using neutron pair distribution function analysis. *Phys. Rev. Lett.* **94**, 147602 (2005).
- Li, F. et al. The origin of ultrahigh piezoelectricity in relaxor-ferroelectric solid solution crystals. *Nat. Commun.* **7**, 13807 (2016).
- Viehland, D., Jang, S. J., Cross, L. E. & Wuttig, M. Freezing of the polarization fluctuations in lead magnesium niobate relaxors. *J. Appl. Phys.* **68**, 2916–2921 (1990).
- Manley, M. E. et al. Giant electromechanical coupling of relaxor ferroelectrics controlled by polar nanoregion vibrations. *Sci. Adv.* **2**, e1501814 (2016).
- Kleemann, W. Relaxor ferroelectrics: cluster glass ground state via random fields and random bonds: relaxor ferroelectrics: cluster glass ground state via random fields. *Phys. Status Solidi* **251**, 1993–2002 (2014).
- Ganesh, P. et al. Origin of diffuse scattering in relaxor ferroelectrics. *Phys. Rev. B* **81**, 144102 (2010).
- James, A. R., Priya, S., Uchino, K. & Srinivas, K. Dielectric spectroscopy of Pb(Mg_{1/3}Nb_{2/3})O₃–PbTiO₃ single crystals. *J. Appl. Phys.* **90**, 3504–3508 (2001).
- Gupta, S. M., Prasad, N. V. & Wadhawan, V. K. Impedance spectroscopy of the relaxor behaviour of P.M.N. and la-doped P.M.N.-P.T. compositions. *Ferroelectrics* **326**, 43–47 (2005).
- Berksoy-Yavuz, A. & Mensur-Alkoy, E. Electrical properties and impedance spectroscopy of crystallographically textured 0.675 [Pb(Mg_{1/3}Nb_{2/3})O₃]-0.325 [PbTiO₃] ceramics. *J. Mater. Sci. Mater. Electron.* **29**, 13310–13320 (2018).
- Bovtun, V. et al. Broad-band dielectric response of PbMg_{1/3}Nb_{2/3}O₃ relaxor ferroelectrics: single crystals, ceramics and thin films. *J. Eur. Ceram. Soc.* **26**, 2867–2875 (2006).

- Irvine, J. T. S., Sinclair, D. C. & West, A. R. Electroceramics: characterization by impedance spectroscopy. *Adv. Mater.* **2**, 132–138 (1990).
- Abram, E. J., Sinclair, D. C. & West, A. R. A strategy for analysis and modelling of impedance spectroscopy data of electroceramics: doped lanthanum gallate. *J. Electroceram.* **10**, 165–177 (2003).
- Kirillov, V. V. & Isupov, V. A. Relaxation polarization of PbMg_{1/3}Nb_{2/3}O₃(PMN)-A ferroelectric with a diffused phase transition. *Ferroelectrics* **5**, 3–9 (1973).
- Egami, T. Microscopic model of relaxor phenomena in Pb containing mixed oxides. *Ferroelectrics* **222**, 163–170 (1999).
- Cabral, M. J., Zhang, S., Dickey, E. C. & Lebeau, J. M. Gradient chemical order in the relaxor Pb(Mg_{1/3}Nb_{2/3})O₃. *Appl. Phys. Lett.* **112**, 082901 (2018).
- M. Eremenko et al. Local atomic order and hierarchical polar nanoregions in a classical relaxor ferroelectric. *Nat. Commun.* **10**, 2728 (2019).
- Krogstad, M. J. et al. The relation of local order to material properties in relaxor ferroelectrics. *Nat. Mater.* **17**, 718–724 (2018).
- Ko, J. H., Kim, D. H. & Kojima, S. Correlation between the dynamics of polar nanoregions and temperature evolution of central peaks in Pb[(Zn_{1/3}Nb_{2/3})_{0.91}Ti_{0.09}]O₃ ferroelectric relaxors. *Appl. Phys. Lett.* **90**, 112904 (2007).
- Otoničar, M. et al. Connecting the multiscale structure with macroscopic response of relaxor ferroelectrics. *Adv. Funct. Mater.* **30**, 2006823 (2020).
- Yan, Z. L., Yao, X. & Zhang, L. Y. Fitting and analyzing the dielectric spectra of Pb(Mg_{1/3}Nb_{2/3})O₃-xPbTiO₃ ceramics and single crystals. *J. Electroceram.* **21**, 275–278 (2008).
- Jonscher, A. K., Holloway, R. & College, B. N. The ‘universal’ dielectric response. III. *IEEE Electr. Insul. Mag.* **6**, 19–24 (1990).
- Jonscher, A. K. The Universal’ dielectric response. II. *IEEE Electr. Insul. Mag.* **6**, 24–28 (1990).
- Jonscher, A. K. The ‘universal’ dielectric response. III. *IEEE Electr. Insul. Mag.* **6**, 19–24 (1990).
- A. K. Jonscher. *Dielectric Relaxation in Solids* (Chelsea Dielectrics Press, London, 1983).
- Jonscher, A. K. Dielectric relaxation in solids. *J. Phys. D Appl. Phys.* **32**, R57–R70 (1999).
- Almond, D. P., West, A. R. & Grant, R. J. Temperature dependence of the a.c. conductivity of Naβ-alumina. *Solid State Commun.* **44**, 1277–1280 (1982).
- Almond, D. P. & West, A. R. Mobile ion concentrations in solid electrolytes from an analysis of a.c. conductivity. *Solid State Ion.* **9–10**, 277–282 (1983).
- Almond, D. P. & West, A. R. Anomalous conductivity prefactors in fast ion conductors. *Nature* **306**, 456–457 (1983).
- Almond, D. P. & West, A. R. Impedance and modulus spectroscopy of “real” dispersive conductors. *Solid State Ion.* **11**, 57–64 (1983).
- Almond, D. P. & Vainas, B. The dielectric properties of random R - C networks as an explanation of the ‘universal’ power law dielectric response of solids. *J. Phys. Condens. Matter* **11**, 9081–9093 (1999).
- Almond, D. P. & Bowen, C. R. Anomalous power law dispersions in ac conductivity and permittivity shown to be characteristics of microstructural electrical networks. *Phys. Rev. Lett.* **92**, 1–4 (2004).
- Bowen, C. R. & Almond, D. P. Modelling the ‘universal’ dielectric response in heterogeneous materials using microstructural electrical networks. *Mater. Sci. Technol.* **22**, 719–724 (2006).
- Aouaichia, M. et al. Understanding the anomalous frequency responses of composite materials using very large random resistor-capacitor networks. *Eur. Phys. J. B* **90**, 39 (2017).
- Osman, R. A. M. & West, A. R. Electrical characterization and equivalent circuit analysis of (Bi_{1-x}Zn_x)_{0.5}(Nb_{0.5}Ti_{1.5})O₇ Pyrochlore, a relaxor ceramic. *J. Appl. Phys.* **109**, 074106 (2011).
- Osman, R. A. M., Masō, N. & West, A. R. Bismuth zinc niobate pyrochlore, a relaxor-like non-ferroelectric. *J. Am. Ceram. Soc.* **95**, 296–302 (2012).
- Ye, Z.-G., Tissot, P. & Schmid, H. Pseudo-binary phase diagram and crystal growth of [PMN]. *Mater. Res. Bull.* **25**, 739–748 (1990).

Acknowledgements

X.V. thanks the European Union’s Horizon 2020 research and innovation programme for a Marie Skłodowska-Curie Individual Fellowship (grant agreement No. 700786). J.R.G. thanks the Engineering and Physical Sciences Research Council (EPSRC, Award Ref 1880882). Z.G.Y. acknowledges the support from the U. S. Office of Naval Research (ONR, Grants No. N00014-16-1-3106 and No. N00014-21-1-2085) and the Natural Sciences and Engineering Research Council of Canada (NSERC, Grant No. RGPIN-2017-06915). A.R.W./X.V. and Z.G.Y. thank IM Reaney who suggested our collaboration.

Author contributions

Z.-G.Y. prepared the PMN crystals, X.V. performed the electrical measurements, J.R.-G. carried out the simulations, A.R.W. conceived the project and wrote most of the manuscript. All authors contributed to discussion and interpretation of the results and approved the final version of the manuscript.

Competing interests

The authors declare no competing interests.

Additional information

Correspondence and requests for materials should be addressed to Zuo-Guang Ye or Anthony R. West.

Peer review information *Communications Physics* thanks Michael Manley and the other, anonymous, reviewer(s) for their contribution to the peer review of this work.

Reprints and permission information is available at <http://www.nature.com/reprints>

Publisher's note Springer Nature remains neutral with regard to jurisdictional claims in published maps and institutional affiliations.



Open Access This article is licensed under a Creative Commons Attribution 4.0 International License, which permits use, sharing, adaptation, distribution and reproduction in any medium or format, as long as you give appropriate credit to the original author(s) and the source, provide a link to the Creative Commons license, and indicate if changes were made. The images or other third party material in this article are included in the article's Creative Commons license, unless indicated otherwise in a credit line to the material. If material is not included in the article's Creative Commons license and your intended use is not permitted by statutory regulation or exceeds the permitted use, you will need to obtain permission directly from the copyright holder. To view a copy of this license, visit <http://creativecommons.org/licenses/by/4.0/>.

© The Author(s) 2022